Proceedings of the Thirty-sixth (2026) International Ocean and Polar Engineering Conference **www.isope.org**
Orlando, Florida, USA, May 31-June 5, 2026

ISBN 978-1-880653-72-2; ISSN 1098-6189

Numerical and Experimental Analysis of Motion Responses for a Research Vessel with a Moonpool in Regular Waves

Bo Han[1], *Decheng Wan*[2,*]

[1] China Ship Scientific Research Center, Wuxi, China
[2] Computational Marine Hydrodynamic Lab (CMHL), School of Ocean and Civil Engineering,
Shanghai Jiao Tong University, Shanghai, China
[*]Corresponding author

ABSTRACT

The moonpool, a vertical shaft connecting the deck to the bottom of a ship, is a critical structure for the deployment and recovery of underwater equipment in various marine engineering vessels and platforms. However, its presence significantly alters the global hydrodynamic performance of the vessel. This study presents numerical and experimental investigation into the motion responses of a research vessel equipped with a moonpool. Numerical simulations covering a range of wave parameters were performed and systematically validated against model test results, showing favorable agreement in predicting the key motion characteristics. The results indicate that waves can modulate the resonant response typically induced by the moonpool by altering the encounter frequency and the energy transfer mechanism, which in some cases leads to amplified motion amplitudes. The opening moonpool involves extra vortex structures, which changes the flow characteristic of the ship and influence the motion response of the ship. This study underscores the significant impact of the moonpool on global motion responses in numerical predictions. The findings offer valuable insights for optimizing moonpool design and enhancing the operational safety of vessels equipped with such structures in realistic sea conditions.

KEY WORDS: Moonpool; motion responses; numerical simulation; model test

INTRODUCTION

The study of moonpool effects on the motion response of research vessels is of paramount importance for ensuring operational safety, mission success, and structural integrity in often harsh and unpredictable ocean environments. A moonpool, a vertical opening through the hull, is a critical feature on many research vessels, serving as a protected launch and recovery site for sensitive equipment like Remotely Operated Vehicles (ROVs), Autonomous Underwater Vehicles (AUVs), coring systems, and deep-sea sensors. However, this very opening fundamentally alters the hydrodynamic characteristics of the vessel. Under wave action, the water column inside the moonpool can enter resonance when the frequency of incident waves matches the moonpool's natural frequency. This resonant fluid motion generates significant dynamic pressure loads on the moonpool walls and internal equipment, exacerbates the vessel's global motions, and can lead to dangerous phenomena such as "green water" ingress or slamming. For research operations, excessive motion compromises the precision of deploying and maneuvering multi-million-dollar scientific payloads, increases the risk of equipment damage or loss, and can force mission delays or cancellations. Furthermore, these dynamic loads contribute to fatigue damage on the hull structure over time.

Fig. 1. “Xuelong 2” polar icebreaker

Consequently, research in this field, as highlighted in the analyzed document, is vital for optimizing moonpool design—considering its shape, dimensions, and potential damping devices—to mitigate these adverse effects. An optimized design minimizes resonant responses, dampens unwanted vessel motions, and enhances the overall stability of the platform. This directly translates to extended operational weather windows, improved safety for personnel and equipment, higher data quality from stable platforms, and reduced long-term maintenance costs.

Ultimately, such research provides the theoretical and practical foundation for designing research vessels that are not only seaworthy but also capable of serving as stable, reliable, and efficient platforms for advanced oceanographic and geoscientific exploration, enabling work in increasingly demanding sea conditions. The document underscores that ignoring the influence of moonpool opening shape is a significant gap; thus, focused research is crucial for developing economical and effective solutions tailored to the specific operational profiles of modern research vessels.

“Xuelong 2” polar icebreaker is China's first domestically built polar research icebreaker. Its most distinctive feature is a centrally located, square moonpool with an opening of 3.2m × 3.2m and a depth of about 10 meters. This system is notable for being the world's first "dry moonpool" on a polar vessel, featuring a weather-tight top cover and a hydrostatically sealed bottom cover to keep the shaft dry when not in use. It is specifically designed for deploying and recovering equipment like CTDs, ROVs, and AUVs safely through the ship's hull in heavy ice or severe sea conditions, avoiding surface ice interference.

Fig. 2. “Explorer III” comprehensive research vessel

“Explorer III”, delivered in December 2024, is China's first comprehensive research vessel capable of global deep-sea exploration and ice-zone manned submersible support. A key technological achievement is its domestically developed, watertight scientific moonpool system, which is the largest of its kind in China with an opening of 6m × 4.8m . This large moonpool enables the deployment of scientific equipment from inside the ship's hull, providing a protected workspace for operations in icy or rough seas and significantly enhancing the vessel's operational adaptability in polar regions.

Fig. 3. “Weilai” deep-sea green intelligent technology test vessel

The "Weilai" is China's first deep-sea green intelligent technology test vessel, delivered in July 2025. A central feature of this 110.8-meter-long, 7,000-ton displacement "mobile laboratory" is its innovative moonpool system located amidships. This rectangular opening, designed as a "water elevator," features a unique track and clamping device system that allows submersibles and other deep-sea equipment to be lowered directly through the ship's hull along guided rails, providing a protected and stable deployment and recovery environment even in rough seas . This system is crucial for its mission as a public testing platform, enabling the real-sea validation of various underwater equipment in depths of 1,000 to 3,000 meters, thereby filling a critical gap in China's deep-sea equipment development cycle .

In terms of the research of moonpool, Senthuran et al. (2020) experimentally and numerically investigates the coupled hydrodynamic responses between a freely floating vessel and moonpools of three different sizes in regular and irregular waves. The key findings are that the moonpool's influence on ship motions (especially heave, surge, and sway) becomes significant with larger moonpools, and that nonlinear effects like secondary resonance and vortex-induced damping at the moonpool entrance are dominant, particularly near resonance. Huang et al. (2021) experimentally investigates the fluid motion characteristics within a recessing-type moonpool with a large aspect ratio. It identifies complex motions like piston and sloshing modes under resonance and evaluates the reduction effectiveness of three damping devices, and finds that these damping devices generally provide good reduction effects, with better performance observed for incident waves of smaller periods. Du et al. (2025) finds that installing a slender moonpool increases ship resistance by over 50% and induces unique high-frequency and low-frequency oscillations that deviate from conventional empirical formulas, with their amplitude and period showing strong dependence on the Froude number. It further reveals that the distinct flow regime inside the moonpool, resembling a hydraulic jump and generating intense periodic waves, is attributed to its large length-to-draft ratio and the significant viscous effects from the sidewalls. And pointed out that modifying the bottom geometry in front of a ship's moonpool (via chamfer, slot, fillet, or combined designs) can significantly alter hydrodynamic performance. Zhao et al. (2025) reveals that the piston-mode resonance of fluid within the moonpool significantly amplifies the vessel's heave motion, with the heave amplitude positively correlated to the dominant frequency peak of the internal fluid. It further finds that the nonlinear higher harmonics excited inside the moonpool cavity produce a distinct "spike" phenomenon, which is uniquely observed in the vessel's roll motion response.

This study conducts a combined numerical and experimental investigation into the motion responses of a research vessel equipped with a moonpool. Numerical simulations, spanning a range of wave parameters, and comparing the motion response of ship with different moonpool status, in order to ensure the mechanism of the influence of moonpool.

EXPERIMENT SETUP

Table 1. The main parameter of the ship model (scale ratio 1:28)

Parameter	Unit	Value
Overall length	m	3.96
Length between perpendiculars	m	3.68
Waterline length	m	3.82
Molded breadth	m	0.71
Draft	m	0.21
Displacement	m^3	0.3183
Center of gravity height	m	0.2807

A model test was conducted in the basin of the China Ship Scientific Research Center, which measures 69 m in length, 46 m in width, and 4 m in depth. The ship model was oriented towards the wave maker, with this direction designated as the positive *x*-direction; the wave damping zone is situated at the rear of the basin. The vertically upward direction is defined as the positive *z*-direction, while the *y*-direction is determined according to the right-hand screw rule. The ship model has a scale ratio of 1:28, and its parameters are detailed in Table 1. The parameters for the operational conditions are listed in Table 2.

Fig. 4. Ship model of the research vessel

Table 2. Parameters of working conditions

Case number	Wave height (m)	Wave length (m)	Moonpool Status
1	0.08	3.82	Open
2	0.08	1.91	Open
3	0.08	0.91	Open
4	0.08	3.82	Close
5	0.08	1.91	Close
6	0.08	0.91	Close

NUMERICAL METHODS

Governing Equations

Assuming the fluid is an incompressible and homogeneous viscous Newtonian fluid, the governing equations are given by continuity equation and Navier-Stokes equations as follows

$$\frac{\partial u_i}{\partial x_i}=0 \tag{1}$$

$$\frac{\partial u_i}{\partial t}+u_j\frac{\partial u_i}{\partial x_j}=-\frac{1}{\rho}\frac{\partial p}{\partial x_j}+v\frac{\partial^2 u_i}{\partial x_j \partial x_j}+f_i \tag{2}$$

where i and j represent the cell address in the *x*- and *y*-direction, respectively, u_i is the velocity component in the x_i-coordinate direction, ρ is the density of the fluid, p is the pressure, v is kinematic viscosity and f_i denotes the body forces such as the gravity force.

Interface Tracking Method

In the two-phase simulations conducted in this study, the free surface is tracked using the Volume of Fluid (VOF) method. This approach primarily relies on the volume fraction, which denotes the volumetric ratio of each grid cell. The volume fraction at the current time step can be updated via

$$\frac{\partial \alpha}{\partial t}+\nabla\cdot\mathbf{U}\alpha+\alpha(1-\alpha)\nabla\cdot\mathbf{U}_c=0 \tag{3}$$

In which $\mathbf{U}_c=\min\left[c_\alpha|\mathbf{U}|,\max\left(|\mathbf{U}|\right)\right]\frac{\nabla\alpha}{|\nabla\alpha|}$, where constant c_α is a compression factor and takes value 1 by default.

Wave Generation

The wave condition in the present work is regular wave, and the Stokes second wave theory is chosen for the wave generation. The theoretical free surface height of the Stokes second wave is

$$\eta=\frac{H}{2}\cos(\theta)+k\frac{H^2}{4}\frac{3-\tanh^2(kh)}{4\tanh^3(kh)}\cos(2\theta) \tag{4}$$

where H is designed wave height; θ is phase of the wave; k is wave number; h is the depth of the wave tank.

In the present work, both wave and current contribute to the main working condition, therefore the influence of current is also demand to be taken into consideration. The horizontal and vertical free surface velocity components are

$$u=\frac{H}{2}\omega\frac{\cosh(kz)}{\sinh(kh)}\cos(\theta)+\frac{3}{4}\frac{H^2\omega k\cosh(2kz)}{4\sinh^4(kh)}\cos(2\theta) \tag{5}$$

$$w=\frac{H}{2}\omega\frac{\sinh(kz)}{\sinh(kh)}\sin(\theta)+\frac{3}{4}\frac{H^2\omega k\sinh(2kz)}{4\sinh^4(kh)}\sin(2\theta) \tag{6}$$

in which, ω is angular velocity of the wave.

NUMERICAL SETUP

Computational Domain

The main parameters of the computational domain is shown in Fig. 5. The size of the whole domain is set as -15 m ~ 12 m, 0 ~ 7 m and -4 m ~ 2 m in *x*, *y* and *z* direction.

As to the boundary condition, the wave generation and inflow is set at the inlet boundary, and the corresponding wave absorption is also set at the outlet boundary. The no-slip boundary condition is adopted to the bottom and the cylinder boundary, the Neumann boundary condition is applied to the atmosphere boundary, and the symmetry boundary condition is imposed on the both sides of the computational domain.

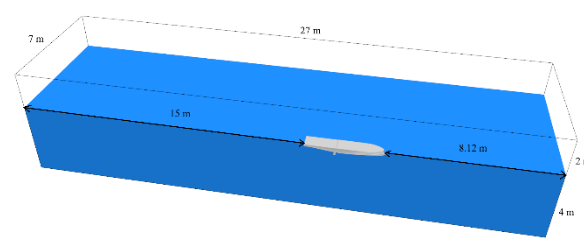

Fig. 5. Computational domain

Computational Mesh

To ensure the execution of a high-fidelity numerical simulation, the utilization of an appropriate computational mesh is crucial. In this study, the overset mesh technique is employed for the numerical simulation.

The background mesh and the overset mesh are generated independently, as depicted in Fig. 6. Overall, concerning the distribution of background cells, the mesh is designed to be denser in regions closer to the free surface to capture the flow field as accurately as possible within the constraints of finite computing resources. Based on some experimental simulations, the cells near the free surface (within the range of -0.06 m $\leq z \leq$ 0.06 m) are specifically refined to a size smaller than 1/40 of the wave height. The background mesh comprises a total of 3,692,998 cells. Additionally, the overset mesh is configured around the ship hull, consisting of 1,765,154 cells.

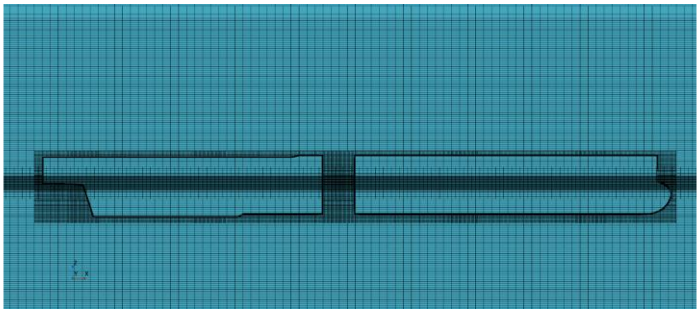

Fig. 6. Overset mesh of the numerical simulation

Mesh Convergence Investigation

The numerical simulation is conducted on 3 sets of meshes with same working condition but the existence of cylinder in the same CFD time of 30 seconds, in order to check out which one fits the simulation best. Table 3 lists the grid sizes and clock time of the 3 sets of meshes from coarse to fine, and Fig. 7 compares the heave historical curves of 3 sets of meshes.

Table 3. Parameters of 3 sets mesh in mesh convergence study

Mesh number	N_t	Δx (m)	Δz (m)	Clock time (s)
1	2.1×10^6	0.1906	0.004	9356
2	5.5×10^6	0.0953	0.002	18571
3	1.4×10^7	0.0477	0.001	47904

In which, N_t is the total cells number of the mesh; Δx is the uniform horizontal cell size of overset mesh; Δz is the uniform vertical cell size of the refinement region around the free surface.

As illustrated in Fig. 7, it is evident that the heave peak of Mesh 1 is marginally lower than those of the other two mesh sets, attributable to numerical dissipation. Following the recommended methodology by Celik et al., the peak values extracted from the heave history curves of the three mesh sets were subjected to a grid convergence index (GCI) analysis, as detailed in Table 4. The grid refinement factor, denoted as r, is set to 2. Through computation, the convergence ratio is found to be less than 1, confirming that the solution exhibits monotonic convergence as the mesh is refined. Additionally, the numerical uncertainty, as quantified by the GCI, diminishes with progressive mesh refinement and remains below 5%. Consequently, the grid configuration and distribution of Mesh 2 are adopted for subsequent numerical simulations and analyses.

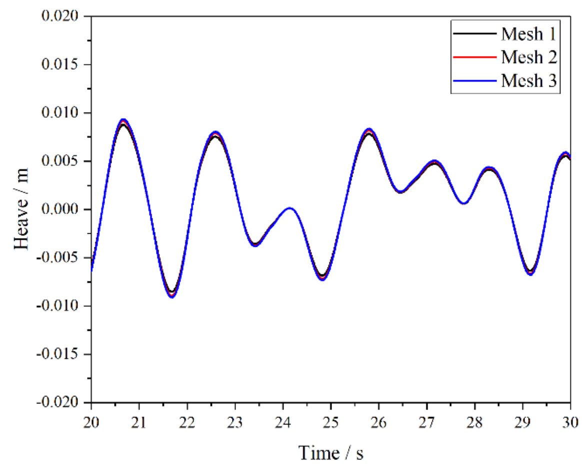

Fig. 7. Heave historical curves of 3 sets of meshes

Table 4. Grid convergence index (GCI) result

Parameter	Value
ε_{12}	-0.00713 m
ε_{23}	-0.00457 m
r	2
Converge ratio	0.641
p	0.642
GCI_{12}	7.142%
GCI_{23}	4.285%

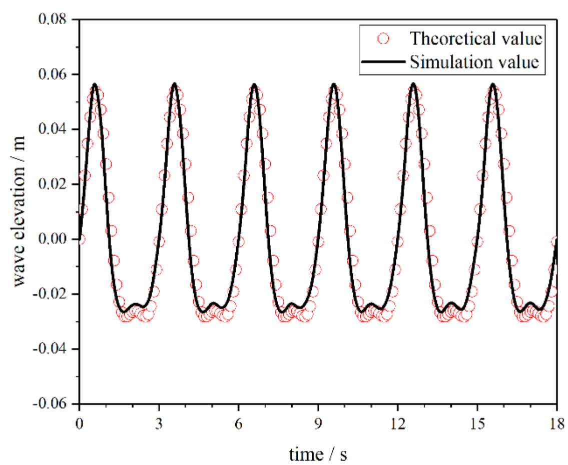

Fig. 8. Wave elevation historical curves of regular wave test and theoretical solution

Wave Validation

Having confirmed the grid convergence of the solution and selected an appropriate grid strategy in the preceding section, which ensures that the numerical simulation yields results with minimal numerical uncertainty, the next step involves validating the wave solution. A regular wave generation test is conducted using the mesh that adopts the aforementioned grid strategy and numerical configuration. The parameters for the regular wave remain consistent with those in Case 1, allowing for the calculation of a theoretical solution. The test results are then compared with the theoretical solution in accordance with Eq. 4, as depicted in Fig. 8. During stable periods, the relative error of the simulated values remains below 3%, thereby confirming the efficacy of the numerical setup and grid adaptation for the current operational conditions.

RESULT AND DISCUSSION

According to the cases conducted in the experiment and numerical simulation, wave length and the moonpool status can be investigated as variables. Subsequently, each of them will be discussed in turn.

Wave Length

The results of heave response in case 1~3 of experiment and numerical simulation is shown in Fig. 9. The vertical axis represents the significant unilateral amplitude value of heave. According to the comparison, results of experiment and numerical simulation are close, the deviations between them are lower than 10%.

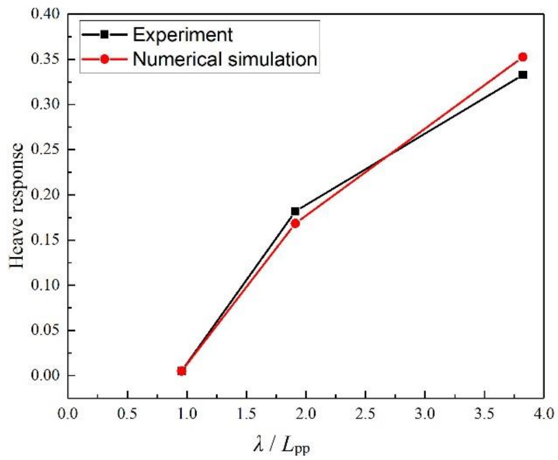

Fig. 9. Heave response in case 1~3 of experiment and numerical simulation

The heave historical curves of ship model and the frequency domain analysis results in case 1~3 are compared in Fig. 10. The results indicates that the heave amplitude increases significantly with the increase of wave length, almost in a proportional relationship. The typical frequence is also varies due to the different wave length, which is identical to the wave-encounter frequence.

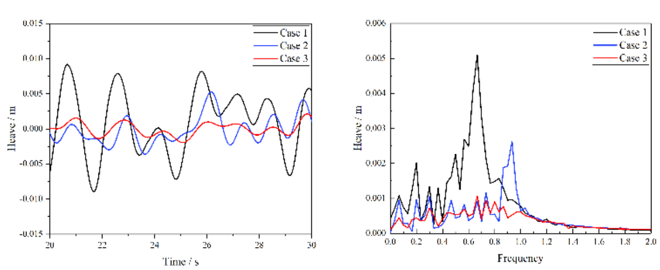

Fig. 10. Heave historical curves and frequency analysis of numerical simulation in case 1~3

Moonpool Status

In order to examine the effects of opening and closing the moonpool on heave motion response, a comparison was made between the heave motion response results of case 1 and case 4, with all other variables held constant. The results are shown in Fig. 11. The graph indicates that in the condition where the moonpool is open, the peak-to-valley values of the heave motion slightly decrease, and the coupling between peaks becomes more pronounced. This may be related to the specific flow structure.

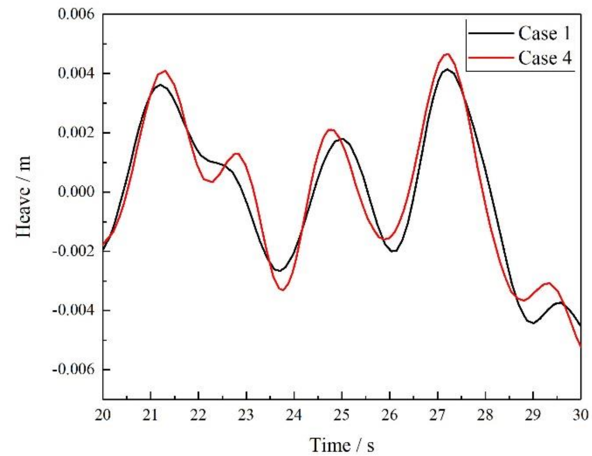

Fig. 11.Heave historical curves in case 1 and 4

The vortex situation at the transverse section calculated using the Q criterion is shown in Fig. 12. It can be observed that obvious vortex structures appear at both the front and rear ends of the lower edge of the moon pool, while the condition of closing the moon pool does not provide the conditions for such flow characteristics. The generation of vortices disturbs the flow structure, further affecting the motion response of the hull.

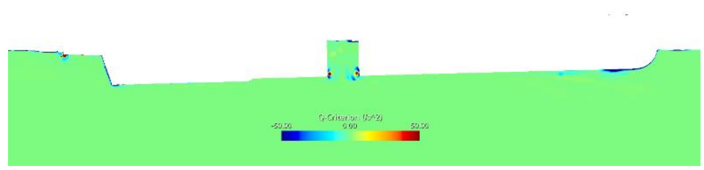

Fig. 12.Vortex situation at transverse section at 25.9 s

CONCLUSIONS

The present study conducted a combined numerical and experimental investigation into the motion responses of a research vessel equipped with a moonpool. The key findings demonstrate that the presence of the moonpool significantly alters the flow structure around the vessel, then the hydrodynamic performance of the vessel is also influenced. Specifically, incoming waves can modulate the resonant fluid motion typically induced within the moonpool by altering the wave-vessel encounter frequency and the associated energy transfer mechanism, which in some scenarios leads to amplified motion amplitudes. Furthermore, the open moonpool introduces additional vortex structures, modifying the local and global flow characteristics around the hull and consequently influencing the ship's motion. The numerical simulations, validated against model tests, successfully captured these key motion characteristics. The research underscores the critical importance of accounting for the moonpool's impact in hydrodynamic predictions and offers valuable insights for optimizing moonpool design to enhance the operational safety and seakeeping performance of such vessels in realistic sea conditions.

REFERENCES

Du, Y, Pan, L, Zhou, W, Cao, L, and Wan, D (2025).“Hydrodynamic performance and wave dynamics in the moonpool of a ship. Part I: Froude number effects on resistance and flow regime, ” *Ocean Engineering*, 342, 122906.

Gaillarde, G, Cotteleer, A (2004). “Water motion in moonpools empirical and theoretical approach.” *Proceedings of the Association Technique Maritime Et Aeronautique*. Paris, France.

Han, B, Zhao, W, and Wan, D (2021). “Numerical study on interaction between focusing waves with fixed cylinder”. *International Journal of Offshore and Polar Engineering*, 31(1), 95-101.

Huang, X, Xiao, W, Yao, X, Gu, J, and Jiang, Z (2021)"An Experimental Investigation on Reduction Effect of Damping Devices for the Recessing Type Moonpool with a Large Aspect Ratio." *J Ship Res* 65, 223–242.

Jing, P, He, G, Yang, K, and He R (2023)"Hydrodynamic Characteristics of a Heave Moonpool with Varied Gap Widths Under Gap Resonance Conditions." Paper presented at the The 33rd International Ocean and Polar Engineering Conference, Ottawa, Canada.

Kawabe, Hiroshi, Kwak, HyunUk, Park, JongJin, and MunKeun Ha. (2010)"The Numerical And Experimental Study On Moonpool Water Surface Response of a Ship InWave Condition." *The Twentieth International Offshore and Polar Engineering Conference*, Beijing, China,.

Pan, C, Li, Z, and Gao, S (2025)"Analysis of the Effect of Different Moonpool Opening Shapes on the Motion Response of Deep-Sea Mining Ship." Paper presented at the The 35th International Ocean and Polar Engineering Conference, Seoul, Korea.

Park, Sun, H, and Seung, H (2025)"Study on the Fluid Impact Force Acting on the Splash Plate Inside the Drillship Moonpool." *The 35th International Ocean and Polar Engineering Conference*, Seoul, Korea.

Senthuran, R, Trygve, K, Bernard, M, and Babak, O (2020). “Coupled vessel and moonpool responses in regular and irregular waves,” *Applied Ocean Research*, 96, 102010.

Sun, J, Sun, S, He, J, and Sun, S "Research on Added Resistance of Improved Configuration Based on Moonpool with Recess." *The 32nd International Ocean and Polar Engineering Conference*, Shanghai, China, June 2022.

Sun, J, Sun, S, Lu, L, and Sun, Z (2023)"Seakeeping Performance Study on a Drillship with Varied Moonpool Configurations Based on Recess-Type Moonpool." *The 33rd International Ocean and Polar Engineering Conference*, Ottawa, Canada.

Tang, Q, Cheng, H, He, X, and Wu X (2024)"Dynamic Simulation of Umbilical Cable Operated in Moonpool Space." *The 34th International Ocean and Polar Engineering Conference*, Rhodes, Greece.

Wang, Y, Zhang, X, Chen, Z, and Yue, J. (2024)"Prediction of Wave-Induced Motion Response for High Sea State Moonpool Salvage Catamaran." *The 34th International Ocean and Polar Engineering Conference*, Rhodes, Greece.

Yu, X, and Zhou, L (2022)"Study on the Resistance Performance of Ships with Moonpool." *The 32nd International Ocean and Polar Engineering Conference*, Shanghai, China,.

Zhimin Zhao, Li Zou, Guoqing Jin, Jiazhao Sun, Zongbing Yu, Zhe Sun, (2025) “Numerical investigation of coupled responses of a mining vessel and moonpool in regular and irregular waves with varying moonpool aspect ratios using SPH.” *Ocean Engineering*, 339(Part2).